Enclosed Pool Fires in Low Ventilation Enclosures: Flame Temperatures and Global Heat Loss Using Gas Analysis

G.E. Andrews, J. Ledger and H.N. Phylaktou
Department of Fuel and Energy, The University of Leeds, Leeds, LS2 9JT, UK

ABSTRACT

Enclosed kerosene pool fires were investigated with ventilation equivalent to normal leakage into a room with the doors and windows closed and air in leakage due to gaps around doors and windows. A 1.9 m^3 enclosed fire test facility with separate air inlet at floor level and fire product outlet at ceiling level was used. A fully heated gas sample system was used, including unburnt fuel analysis, as total hydrocarbons are required as well as CO to determine the combustion efficiency and the air/fuel ratio by carbon balance. This air /fuel was used to determine the adiabatic mean flame temperature of the fire as a function of time as well as the entrained air mass flow rate. The adiabatic temperature was compared with the measured flame temperature and it was shown that the time to peak temperature was the same. The temperature difference was used to determine the global heat loss to the enclosure walls as a function of time. The peak heat transfer per unit wall surface area was 6 kW/ m^2 for the highest ventilation rate. The global heat transfer to the enclosure was 70-80% of the heat release at the peak fire intensity for three ventilation air flow rates. NOx concentrations were also determined and the rate of formation of NOx was used to compute the temperature of the hot zone that formed the NOx. This temperature was shown to increase very rapidly after the start of the fire to a maximum of approximately 1500K for all three ventilation rates. The size of this hot zone was taken as a cylinder of vertical height equal to a free pool fire flame height and diameter. The surface area of this at 1500K was shown to account for the measured global heat transfer.

KEYWORDS: Compartment fire temperatures, pool fires, fire heat transfer, NOx.

INTRODUCTION

The development of fires in rooms with good compartmentation and very low air leakage rates is studied in this work using pool fires. The ventilation rate to the fire is quantified by an air inlet area coefficient, K_{in} . This is the air in leakage open area divided by the cross sectional area of a cubic room of equivalent volume to the test room. This allows any air leakage path to be considered and is independent of the shape of the enclosure. For a typical 3 x 5 x 2.5 m^3 room with a single door and normal air leakage paths around the door (1), the range of values of K_{in} are from 0.09% to 0.6%. Normally higher air leakage paths greater than 1% would only occur because a window or door had been left open.

The present work investigated enclosures with values of K_{in} of 0,. 0.11% and 1%. There have been few previous studies of fires in compartments with such restricted air inlets. The lowest K_{in} used in the literature for pool fires was 1.55% in the work of Audouin et al. (3), whereas the highest K_{in} used in the present work was 1.0% (1). The large scale enclosed pool fire work of Chamberlain (4) had very large ventilation openings and K_{in} values of 9.43% and 26.3% (1). Gottuk et al. (5,6) used a K_{in} of 4.4% in a similar test facility to the present. Fleischman and Parkes (7) used a ventilated enclosure with a K_{in} of 9.2% (1) and Peatross and Beyler (8) had a test facility with three values of K_{in}, 1.7, 2.7 and 6.8%. Most of this previous work investigated fires in enclosures equivalent to the case

with a window or door open at the start of a fire. The present work was designed to simulate enclosed fires with the doors and windows closed and leakage air due to gaps around doors and windows (1).

Pool fires were used for two main reasons. Firstly, there is a requirement from offshore fire hazard evaluation work to understand more about hydrocarbon pool fires in enclosures and the production of toxic products (4). Secondly, pool fires are reproducible fires and repeat tests at differen air ventilation rates or hydrocarbon volatility can readily be undertaken. They represent real fires in enclosures with a time development of the heat release rate and a gradual increase with time of the external air entrainment.

EXPERIMENTAL TECHNIQUES

A 1.9 m^3 internal volume enclosed fire test facility, shown in Fig.1, of external dimensions 1.4m x 0.96m x 1.5m was used with a 200mm square kerosene pool fire. The fire load was supporte on a fire board base which rested on 3 load cells mounted in the air supply plenum. The pool fire rate of weight loss was used to determine the heat release in the fire as the product of the mass loss rate an the fuel calorific value. The walls were steel plate lined with a 25mm thick high temperature insulatin fire resistant board. There was a separate air inlet at floor level and fire product exit at ceiling level, as shown in Fig.1. This enclosure had an initial air mass content of 2.32 kg at ambient conditions (densit 1.2 kg/m^3). The air inlet and the fire product outlets were arranged to be at the periphery of the fire enclosure at floor and ceiling level respectively. This was to minimise any fire shape distortion due to the air flow inlet or product exit. This design was adopted so as to make the test situation amenable to mathematical modelling. The air inlet to the fire enclosure was through a 250mm deep plenum chamber under the fire test volume. There were four 25mm wide slots that ran along each of the four sides of the plenum chamber roof, which also formed the steel floor of the fire enclosure. The area of these slots (0.1 m^2) was always greater than the air inlet area so that the air flow was controlled at the inlet to the plenum chamber. Three air supply inlet sizes were investigated, no air, a 46mm diameter hole (0.0017m^2) and a 0.016 m^2 rectangular hole. The air inlet vent coefficient K_{in} was 0, 0.11% and 1.0% for the three air inlet conditions studied.

The fire enclosure had a flat steel roof with no insulation and the fire products were drawn off by natural convection at the edges of the roof. The hot fire product gases flowed into a collection volume above the steel roof where they were extracted through a 150mm diameter duct into a dump volume where a large hood and extraction system transported the fire products through a suction fan and discharged them through a 10m high chimney. A water cooled multi-hole 'X' gas sample probe, with 40 sample holes on centres of equal area, was inserted in the fire ceiling outlet duct to obtain a mean gas sample from the ceiling layer without any external air entrainment. This has been shown to give very similar gas composition results to that of the ceiling layer. However, it was a better mixed sample and was a more reliable measurement of the mean gas composition of the ceiling layer. The ga sample was transferred to the analysers through 180C heated teflon sample lines, 180C heated sampl pump and filter and heated hydrocarbon and nitric oxide wet gas analysis. Part of the sample was cooled to 2C to remove the water vapour using a thermoelectric cooler with continuous condensed water removal. This dry sample was analysed for carbon monoxide, carbon dioxide and oxygen. The gas analysis was used to determine, by carbon balance, the fire air/fuel ratio by mass. The fire combustion efficiency was determined from the energy content of the carbon monoxide and hydrocarbons. Both the air/fuel ratio and the combustion efficiency were determined as a function of time.

HEAT RELEASE RATE FOR THREE VENTILATION RATES

The heat release rates is shown as a function of time in Fig 2 for the highest ventilation rate (K_{in}=1%), the results have been corrected for the combustion efficiency which was a significant correction at the highest heat release rate. The strong influence of the ventilation rate on the efficiency corrected heat release rate is shown in Fig. 3. The highest heat release rate of 70kW was found for th highest air ventilation (K_{in}=1%). The results with the no external air ventilation show that the flame

went out with only 20% of the fuel load burnt and this occurred after about 250s. For both of the ventilated fires all the fuel load was burnt out. The lower ventilation rate had all the features of a steady state fire with a near constant heat release rate of about 15 kW from 100s to 900s. All three fires had a similar heat release rate in the first 100s, indicating that the air in the enclosure dominated the fire propagation in this period.

The maximum heat release rate for the highest ventilation in this work was 70kW, which converts to 1.75 MW/m^2 of pool surface area. or 52.2 kw/m^3 of enclosure volume. For comparison the mean heat release rates in the large scale tests of Chamberlain (4) using diesel pool fires were from 0.82 to 1.81 MW/m^2 of pool surface area (using a CV of 43 MJ/kg). On a chamber volume basis the average heat release in the work of Chamberlain was from 36 to 168 kw/ m^3 and the present peak heat release rates (52 kw/ m^3) are within this range. Audouin (3) also reported the mean heat release rate for enclosed pool fires and this was 0.8 MW/ m^2 of pool area or 8.53 kw/m^3. Thus the maximum heat release per unit pool surface area or per unit enclosure volume in the present work with the highest ventilation rate was similar to that in the much larger experiments of Chamberlain (4) and larger than that in the work of Audouin (3).

For kerosene pool fires in the open with a pool diameter of 0.2m the heat release rate is 0.86 MW/m^2 but this increases to 1.68 MW/m^2 for 2m pools (18) and for pools in the 20-80m diameter range the heat release is 2.58 MW/m^2 (19). For comparison with the present work using 0.2m pool size the relevant open pool fire heat release rate is 0.86 MW/m^2 and the present maximum heat release is 1.75 MW/m^2 The increase in the heat release rate is due to the radiation feedback to the pool from the enclosure walls. In large diameter open pool fires the same effect occurs from internal radiation from soot in the flame to the pool surface. Heselden et al (20) gave a criterion for ventilation control that involved a fire load greater than 150 kg/m^2 of inlet area. In the present work this parameter was 176.5 kg/m^2 for K_{in}=0.11% and 37.5 kg/m^2 for K_{in}=1.0% and both experiments were clearly ventilation controlled.

GAS COMPOSITION RESULTS AND AIR/FUEL FOR THREE VENTILATION RATES

The oxygen, carbon dioxide, carbon monoxide and total hydrocarbons volumetric concentrations in the fire enclosure ceiling exit plume are shown as a function of time in Fig. 4 for the three air ventilation cases. These show that the first 200 seconds of all the fires were similar and hence independent of the ventilation rate. This early phase of the fires was dependent on the air already in the enclosure. All four gases behaved in the same way in this period, at the end of which the oxygen was depleted to 15.5% and the CO was 0.1%. For the case with no air ventilation the pool fire went out through lack of oxygen. The 15.5% oxygen at extinction is close to the oxygen flammability limit for CO2 inerting, which is 14.4% for higher hydrocarbons (21). For the ventilated fires the oxygen continued to be depleted at the ceiling level, as the pool fire entrained air at floor level which sustained the flame. However, the higher oxygen supply increased the heat release rate, which consumed more oxygen. The heat release for the highest air ventilation reached a maximum at 350s into the fire and this was accompanied by a reduction in the oxygen level below that of the intermediate air ventilation case. The CO and UHC emissions suddenly increased in this period of maximum heat release. For the highest ventilation the UHC levels were too high for the instrument to resolve. This indicates that the fire was air starved and would be at its richest equivalence ratio, as shown below. The intermediate air ventilation had a steady heat release rate throughout the fire, after the first 100 seconds and the air supply was just sufficient to match that required for the 15 kW heat release. Fires require 3 kg of air per MJ of heat released and hence the 15 kW fire required an air consumption of 0.005 kg/s. This was the air entrainment calculated for a mean fire temperature of 200C and a vertical height of 1.5m above the air inlet. This fire did not become highly air starved as the CO emissions did not increase beyond 0.3% and the UHC emissions remained relatively low.

The gas analysis results were used to compute the mean ceiling level air/fuel ratio, using the carbon balance method. The results are shown in Fig. 5 and for all ventilation rates the fire mean

equivalence ratio was lean. However, for the maximum ventilation rate the mean equivalence ratio was close to stoichiometric but was never a rich mixture overall. This contrasts with the work of Gottuck e al (5,6) who used a similar test rig to the present but with a more volatile fuel and they reported the mean fire equivalence ratio being richer than stoichiometric at the maximum heat realease rate.

MEAN CEILING FLAME TEMPERATURE

The measured mean temperatures 70mm below the ceiling were determined from an array of Type K 3mm diameter mineral insulated thermocouples with an exposed junction 1mm diameter bead. The temperature profile was fairly uniform in the central region and the mean of four thermocouples was used as the ceiling layer mean temperature. The measured temperatures were uncorrected for radiation losses. The work of Blevins (9) shows that the error in the present circumstances could be of the order of 5%. Measurements of the wall temperatures and gas velocities in the thermocouple region would be required to carry out the full correction and this data was not available.

The maximum ceiling layer temperatures are shown as a function of time in Fig. 6 for the three ventilation conditions. The peak temperature increased markedly as the ventilation rate was increased, from 180C for no ventilation to 280C for K_{in} = 0.11% and 500C for K_{in} = 1.0%. The results are simila to those of Peatross and Beyler (8) for diesel pool fires, in a much larger enclosure than was used in th present work. They used a similar relative pool size and a minimum air inlet ratio, K_{in}, of 1.7% which was close to the present maximum of 1.0%. The pool surface area to floor area ratio used by Peatross and Beyler (8) were 2.7% and 4.9%, similar to the 3.0% used in the present work. The peak ceiling layer temperature using diesel at the lowest ventilation rate was 225C and 300C respectively for the two relative pool sizes. These are lower than the present temperature of 500C for the nearest equivaler conditions. This could reflect greater heat losses from the diesel pool fires due to the greater generatior of soot. Also the enclosure was constructed of steel plate, which would maximise the heat losses.

NOx FORMATION AND TEMPERATURE REQUIRED TO GENERATE THE NOx

The NOx concentrations, measured using a chemiluminescence analyser (Signal Instruments)with 0.1ppm resolution and 3% accuracy, are shown in Fig. 7 for the three air ventilation conditions. These show a very low level of NOx for the test with no air ventilation and an increasing NOx level as the ventilation was increased. Comparison with Fig.6 shows some similarities with the mean ceiling temperature. The peak NOx coincided with the peak mean temperature, in terms of the time to reach the peak temperature and NOx. For the intermediate ventilation, the NOx continued to increase at a decreasing rate until it reached a maximum just before the fire exhausted the fuel. The results in Fig.7 were smoothed and differentiated over one minute averaging periods to determine the rate of NOx formation. This was used to determine the flame temperature that had generated the NOx.

The main formation of NOx was by the thermal mechanism which involves the reaction between atomic oxygen and nitrogen at high temperatures. This has been extensively studied in relatio to combustion generated NOx and the rate of formation of NOx is given by (10):

$$\frac{d[NO]}{dt} = 1.4\times10^{17} T^{-1/2} \exp\left(\frac{-69{,}460}{T}\right)[O_2]^{-1/2}[N_2] - 10^{7} T^{-1/2} \exp\left(\frac{-46{,}900}{T}\right)[NO]^2[O_2]^{-1/2} \text{ mol cm}^{-3}\text{s}^{-1} \qquad (1)$$

This equation was used with the measured values of the rate of formation of NOx and the measured oxygen to determine the fire hot zone mean temperature. It should be emphasised that the rate of formation of NOx is very low compared to that in furnace burner flames where NOx formation rates are in the region of 1 - 100 ppm/ms depending on the temperature. Fig. 7 shows that the maximum formation rate was 0.1 ppm/s and the minimum was 0.025 ppm/s. The isothermal residence time (fire volume divided by the volumetric air flow rate) was 47s for the fastest burning fire and longer for the lower ventilation rates. The fire flame temperatures corresponding to the thermal NOx based on Eq. 1, are shown in Fig.8 for the three air ventilation rates. This temperature increased rapidly after the start of the fire, much more rapidly than did the measured temperature or the adiabatic mean temperature discussed below. At all three ventilation rates the temperature from the NOx measurements was about 1500K and the influence of the ventilation was a maximum difference of 75C. Comparison of Fig.8

with Fig.6 shows that the NOx was created in a zone that was at a much higher local temperature than the mean fire ceiling temperature. A thermocouple placed 100mm above the pool for the intermediate ventilation situation showed a temperature 200C higher than the ceiling temperature. This indicates that the pool fires in this work did not involve flame impingement on the ceiling.

These results indicate that the hot zone that creates the NOx is increasing in size as the fire develops and is surrounded by a cooler region, with which it mixes in the ceiling layer to yield the measured mean temperature. In the present work, this cooler region may be enhanced due to the air admission at the periphery of the enclosure floor. The hot zone thus becomes hot because the local mean air/fuel ratio is richer than the overall mean air/fuel ratio measured at the enclosure exit. This hot zone will generate most of the radiative heat losses to the walls. The size of this hot zone is estimated below based on the assumption of the radiation received by the walls being dominated by the flame hot zone radiation. The size of this hot zone was calculated on the basis of the measured average heat transfer rate to the walls.

ADIABATIC FLAME TEMPERATURES BASED ON THE GAS ANALYSIS BASED AIR/FUEL

The adiabatic flame temperatures for the air/fuel ratios in Fig. 5 were calculated using thermodynamic data for kerosene (10) and was corrected for the combustion efficiency, based on the energy content of the CO and UHC (2). The resultant temperatures are shown in Fig.9 for the three air ventilation rates. For the highest ventilation the temperature shows a sudden increase of about 50C at around 500s. Fig.4d shows that between 350 and 500s the hydrocarbon analyser went off scale. It was estimated by extrapolation that the maximum UHC was 2%. A consequence of this was that the air/fuel ratio was computed to be leaner than it was and the adiabatic temperature was then low. Thus the 'missing' UHC between 350 and 500s resulted in an under-prediction of the adiabatic temperature.

Figures 10-12 compare the three fire temperatures for the three ventilation rates. The peak adiabatic temperature occurred at the same time as the peak mean ceiling temperature and hence the mean temperature dependence on time is controlled by the fire global equivalence or air/fuel ratio. These results indicate that the local hot zone that generates the NOx grows with time and fills a larger proportion of the fire volume until at the peak of the fire intensity the proportion of the enclosure volume occupied by the hot zone is at a maximum. This hot zone is subject to radiative and convective heat losses and its temperature is below the mean adiabatic.

GLOBAL HEAT TRANSFER TO THE ENCLOSURE WALLS

The difference between the mean outlet gas adiabatic temperature and the measured ceiling temperature is due to heat losses from the fire to the enclosure walls. The heat loss as a fraction of the heat release is shown in Fig.13 for the three ventilation conditions (11). The heat loss per unit enclosure wall area (8.12 m^2) is shown in Fig. 14. An alternative method for deriving the heat loss is simply to deduct the energy flow in the ceiling layer from the heat release rate and this produces very similar results to those in Fig.13.

The peak global heat transfer to the wall is shown in Fig.14 to be 1.0, 1.5 and 6 kW/ m^2 for the three ventilation rates. The heat transfer to the floor was measured by Luo and Beck (12) for a polyurethane slab burning in a 20.7 m^3 enclosure. The initial air/fuel by mass was 8.0 and K_{in} was 26%. The measured heat radiated to the floor was a maximum of 10 kW/ m^2 for a short period. These results are similar to the global wall heat transfer in Fig. 14.. The radiation measured in the large scale pool fire tests of Chamberlain (4) was very high at 300 kW/ m^2 (middle of one wall) and 220 kW/ m^2 (ceiling above the pool) but the fire duration and shape of the total heat flux to the test wall was similar to the present work. Chamberlain also found the heat flux was smaller at the bottom of the walls. The fire temperatures were much higher (1200C) in this work, due to the pool flame hot zone impinging on the ceiling and hence radiative heat transfer was much greater.

The large fractional heat losses in Fig.13 show that 70 - 80% of the heat released was lost from the fires into the enclosure walls. Gross and Robertson (13) studied global heat losses in an enclosed

fire of fibreboard cribs in enclosures of three difference volumes with K_{in} from 0.5% to 25% in each enclosure. For a K_{in} of 1% the fire temperature in the ceiling area was about 350C for the smaller two volumes (0.009 and 0.22 m^3) and 700C for the 6 m^3 fire enclosure. For all the fire volumes the mass burn rate and hence heat release was a near linear function of the air ventilation. For the largest enclosure they showed that the heat transferred to the enclosure walls varied from 80% of the heat released at low ventilation to 50% at high ventilation. Their work at low ventilation was very similar to the highest ventilation of 1% in the present work, with a similar 80% heat loss.

The local hot zone temperature, T_1, derived from the NOx results may be used to estimate the size of the hot zone necessary to yield the measured surface average heat transfer, assuming that radiative heat losses dominated the fire heat transfer. The heat transfer from the flame of surface area, A_1, to the enclosure surface area, A_2 (8.12 m^2), is given by (14)

$$Q/A_2 = e_{net}\,\sigma\,[T_1^4 - T_2^4]\ kW/m^2 \qquad (2)$$

where $e_{net} = 1/[(A_2/e_1 A_1) + 1/e_2 - 1]$

T_1 = The fire hot zone temperature from the rate of formation of NOx

T_2 = The enclosure wall temperature

e_1 = The fire hot zone flame emissivity

e_2 = The enclosure wall emissivity

σ = The Stefan-Bolzman Constant = 5.6697×10^{-8} $W/m^2 K^4$

This equation ignores any contribution from radiation emittance and absorption between the flame radiation and the walls and it cannot be applied to situations where the flame fills the enclosure. In the present work much of the data required to evaluate Eq.2 accurately is not known; T_2, e_1 and e_2. However, the enclosure walls were black with soot deposits and the enclosure itself was a good approximation to a black body, so that it is reasonable to take e_2 as unity. Also as $T_1 >> T_2$ it is reasonable to ignore the value of T_2. The maximum wall temperature for the highest ventilation is unlikely to be above 500K as the peak gas phase temperature in the ceiling is only 773K. The radiation from the wall at 500K is only 1% of the flame radiation at the 1500K temperature in Fig.5. Thus it is reasonable to ignore the radiation from the walls. With these assumptions Eq.2 simplifies to Eq. 3.

$$Q/A_2 = e_1 (A_1/A_2)\,\sigma\,T_1^4\ kW/m^2 \qquad (3)$$

Values of $e_1 (A_1/A_2)$ are given in Table 1 for the three ventilation rates and the peak values of the hea transfer per enclosure surface area in Fig.14. The only unknown now is the term $e_1 A_1$. The hot zone surface area, A_1, was evaluated on the basis that the pool fire flame height is the same as for a free flame. The correlation of Heskestad (15, 16) for the free flame height was used, this gives the flame height as a function of the heat release rate (1). The pool fire hot zone was assumed to be a cylinder of equivalent cross sectional area to the pool area (0.04 m^2) and a height of the flame height. Table 1 shows the computed flame height and the associated hot zone volume as a % of the fire enclosure volume. These results show that the present pool fires were relatively small and the enclosure surface area much larger, so that the assumptions in the use of Eq.3 are valid. The pool fire flame did not impinge on the enclosure ceiling. The values of the flame surface area in Table 1 allow the hot zone emissivity, e_1, to be evaluated and these are given in Table 1. This computation assumes that radiation from outside of the hot zone is negligible.

It may be shown that the other major source of radiative heat transfer is from the ceiling layer at the temperatures in Fig.6. Calculations for the maximum ceiling layer radiation to the wall by the above method and using the emissivities in Table 1 show that at the highest ventilation and the maximum ceiling temperature the radiated heat was only 10.2% of that measured as the global heat transfer to the walls. For the lower ventilation the equivalent figure was 8.75% and for no ventilation it was 5.5%. These heat transfer rates are not negligible and the wall heat transfer from the hot zone is thus reduced and this will alter the emissivity calculations. The corrected emissivities are listed in Table 1.

Table 1 Size of the pool fire hot region

K_{in} %	e_1A_1/A_2 %	Flame Height for Dia 0.226m m	A_1 m^2	Flame Vol. / Enc. Vol %	e_1	e_1 Corrected for ceiling radiation	e_1 Corrected for fire dia.=0.6 pool diameter
0	0.35	0.46	0.363	0.96	0.079	0.074	0.11
0.11	0.51	0.51	0.401	1.07	0.10	0.094	0.14
1.0	1.76	1.05	0.784	2.20	0.18	0.17	0.27

The values of the hot zone emissivity in Table 1 increase with the ventilation, this is due to the increase in the global equivalence ratio and the associated increase in soot concentrations (2). The emissivity of luminous flames may be estimated from Kirchoff's law (16) and the procedures outlined by Drysdale (16). Using the K value for diesel and an equivalent beam length of 0.73 the pool diameter yields an emissivity of 0.07, which is comparable with the values in Table 1 for $K_{in} = 0$. However, Rasbach (16,17) measured the emissivity for kerosene pool fires of 0.3m diameter as 0.37. This is considerable higher than the values in Table 1. They also determined the pool fire plume diameter to be 60% of the pool diameter, whereas a pool fire plume diameter the same as the pool diameter has been assumed in the above calculations. The above calculations were repeated with a pool fire plume diameter 60% of the pool diameter. This resulted in a lower hot zone surface area and an increase in the predicted emissivity as shown in Table 1. These emissivities are still below that measured by Rasbach (16,17). This could be because their measured flame temperature for kerosene was 1263K compared with 1500K in the present work using the NOx rate of formation technique. The higher temperature in the present work was due to the enclosed fire configuration with reduced air entrainment into the plume together with enhanced soot oxidation rates at the higher temperature which will give a lower emissivity.

These results put a more quantitative basis to the qualitative arguments above in relation to the flame hot zone that gave rise to the NOx formation that was measured. A key input to the above calculations was the temperature of the hot zone computed from the rate of formation of NOx in Fig.7. The NOx increased with time for each fire and increased with air ventilation, but the zone generating the NOx remained at approximately the same temperature, 1500 - 1600K. The increase in NOx with time was due to the increase in the size of the hot zone as the fire developed, which gave a longer residence time at the high temperature. The increase in the size of the zone with ventilation was due to the increased mass burn rate (1, 2) which increased the enclosure mean ceiling temperature. This is the temperature after the hot zone has mixed with the cooler surrounding air. For the highest ventilation in the present work, it was estimated that the hot zone occupied 2.2% of the fire enclosure volume. For increased ventilation this would increase until the hot zone occupied all of the enclosure. This was found by Chamberlain (4) for very high ventilation rates and a large pool size. The peak enclosure temperature was close to that of the hot zone in the present work. The pool sizes in the work of Chamberlain were 17 and 35% of the enclosure floor area, compared with 3.0% in the present work. The free flame height for their pool size was greater than the enclosure height, 5.5m for a height of 3.91m. This would lead to flame impingement on the ceiling and the continuation of the flame development along the ceiling with resulting high ceiling temperatures. This results in a fully developed fire with all the enclosure volume at a high temperature as found by Chamberlain for the highest pool fire area. Similar results were found by Gross and Robertson (13) with a maximum enclosure temperature of 1050C for very large enclosures with a high ventilation. This is lower than the temperatures measured by Chamberlain (4) and the hot zone temperature in the present work. However, they used wooden cribs where the peak flame temperature is lower than for the pure hydrocarbon fires used in the present work and in the work of Chamberlain.

Chamberlain (4) measured the vertical temperature profiles in their enclosure, but at a location well to one side of the pool fire plume. In the present work the vertical temperature profiles were not measured. Peatross and Beyler (8) measured vertical temperature profiles for enclosed pool fires with

the measurement location in the corner of the enclosure with a central pool fire. Audouin et al. (3) measured several vertical temperature profiles in a pool fire with a large enclosure. However, their reported vertical profile was well away from the vicinity of the pool fire. They also measured the temperature profiles as a function of time for a series of thermocouples 1.25m from the floor in the 2.5m enclosure. This included thermocouples in the pool fire plume directly above the pool. This showed a 1000C peak temperature 1.25m above the pool compared with a ceiling layer mean temperature of 600-700C. This high temperature region was only present in the region of +/- 1m from the centre line of the 1m diameter pool and then only for the first 300s of the fire. Further work is required with detailed temperature profiles in the region of the pool fire plume to identify the local high temperature burning region that is postulated to give rise to the NOx formation and the bulk wall radiation discussed in this work.

CONCLUSIONS

Kerosene pool fires were investigated in an enclosure with very low air ventilation rates, equivalent to conditions in rooms with the doors and windows closed.

The mean fire outlet gas analysis was used to determine by carbon balance the air/fuel ratio by mass, together with the combustion efficiency. These measurements were used to calculate the adiabatic mean flame temperature as a function of time in the pool fire. These temperature-time results were very similar in shape to the measured ceiling temperatures, indicating that the ceiling temperatures were dependent on the global equivalence ratio.

The difference between the adiabatic temperature and the measured temperature for enclosed pool fires was used to compute the global heat loss to the fire enclosure walls. This had a peak value of 6 kW/m^2 for the highest ventilation rate. The pool fire was shown to transfer 70-80% of the heat release as heat losses to the enclosure walls.

NOx measurements were used to deduce the temperature of the zone that created the NOx from the rate of NOx formation and the oxygen concentration. This was determined to be between 1225 and 1300C and was not strongly dependent on the ventilation of the fire. The profile of this temperature with time was completely different to the measured temperature profile in the ceiling layer which was also at a much lower temperature. This hot zone was created rapidly within 50s of the start of the fire. It was shown that the size of this zone could be estimated using the bulk surface average heat transfer and the hot zone peak temperature as the main radiation source, with the flame emissivity and surface area as the unknown. The pool fire height was estimated using correlations for the height of free pool fires and these were lower than the enclosure height. This enabled the pool fire surface area to be computed with the assumption that the flame shape was a cylinder whose diameter was related to the pool diameter. Thus, it was possible to estimate the flame emissivity needed to achieve the determined heat loss rate to the enclosure walls. The flame emissivities that were predicted were within the range of reported values for similar fires and increased with the ventilation rate due to the richer global combustion higher soot formation.

ACKNOWLEDGEMENTS

We thank the University of Leeds for an academic development grant to build the enclosed fire test facility. J. Ledger is supported by an EPSRC studentship. The gas analysis equipment was provided by the EPSRC from a series of research grants to G.E. Andrews on Diesel engine particulate emissions.

REFERENCES

1. BS 5588:Part 4:1998, Fire precautions in the design, construction and use of buildings. Code of practice for smoke control using pressure differentials
2. Andrews, G.E. , Collins, P., Ledger, J. and Phylaktou, H.N., Enclosed pool fire stoichiometry and the determination of air consumption and combustion efficiency, Paper submitted for publication 1998.
3. Audouin, L., Such, J.M., Malet, J.C. and Casselman, C., A real scenario for a Ghosting Flame, Proc. 5th Int. Symp. On Fire Safety Science, pp. 1261-1272, 1997.
4. Chamberlain, G.A., Trans. IChemE, Vol.74, Part B, pp.81-87, 1996.

5. Gottuk, D.T., Roby, R.J. and Beyler , C.L., A study of carbon monoxide and smoke yields from compartment fires with external burning, 24th Symp. (Int.) on Combustion, pp. 1729-1735, 1992.
6. Gottuk, D.T., Roby, R.J., Peatross, M.J. and Beyler, C.L, J. Fire Prot. Engr., 4, pp.133-150, 1992.
7. Fleischmann, C.M. and Parkes, A.R., Effects of Ventilation on the Compartment Enhanced Mass Loss Rate, Proc. Fifth International Sump. On Fire Safety Science, pp.415-426, 1997.
8. Peatross, M.J. and Beyler, C.L., Ventilation effects on compartment fire characterisation, Proc. 5th Int. Symp. On Fire Safety Science, pp. 403-414, 1997.
9. Blevins, L.G., A new perspective on thermocouple behaviour in room fires, NIST, 27th International Combustion Symposium 1998.
10. Walsh, P.P and Fletcher, P., Gas Turbine Performance, Blackwell Science, 1988.
11. Blair, G.P. , Two Stroke Engines, SAE, 1991.
12. Luo, N. And Beck, V., Stoich. Combustion Model with Oxygen Threshold Improved Predictions for Fire Simulation, Fifth International Symposium on Fire Safety Science, pp. 559-570, 1997..
13. Gross, D. And Robertson, A.F., Experimental fires in enclosures, Tenth International Symposium on Combustion, pp.931-942, 1965.
14. Field, Gill, Morgan and Hawksley, Combustion of Pulverised Coal, BCURA, p.99, 1967.
15. Heskestad, G., Peak gas velocities and flame heights of buoyancy controlled turbulent diffusion flames, 18th Symposium International on Combustion pp. 951-960, 1981.
16. Drysdale, D., An Introduction to Fire Dynamics, Wiley, 1994.
17. Rasbach, D.J., Rogowski, Z.W. and Stark, G.W.V., Fuel, Vol.31, pp.94-107, 1956.
18. SFPE Handbook of Fire Protection Engineering, p.3.3, 2nd Edition,1995
19. J.G. Quitiere, Pool Fires: A Review, Blast and Fire Protection Eng. Project for Topside Structures, Steel Construction Institute, 1991.
20. Heselden, A.J., Thomas, P.H. and Low, M., Fire Tech., Vol.6, p.123, 1970.
21. Lewis, B. and Von Elbe, G., Comb., Flames and Explosions of Gases, 2nd Edition, AP, p.698, 1961

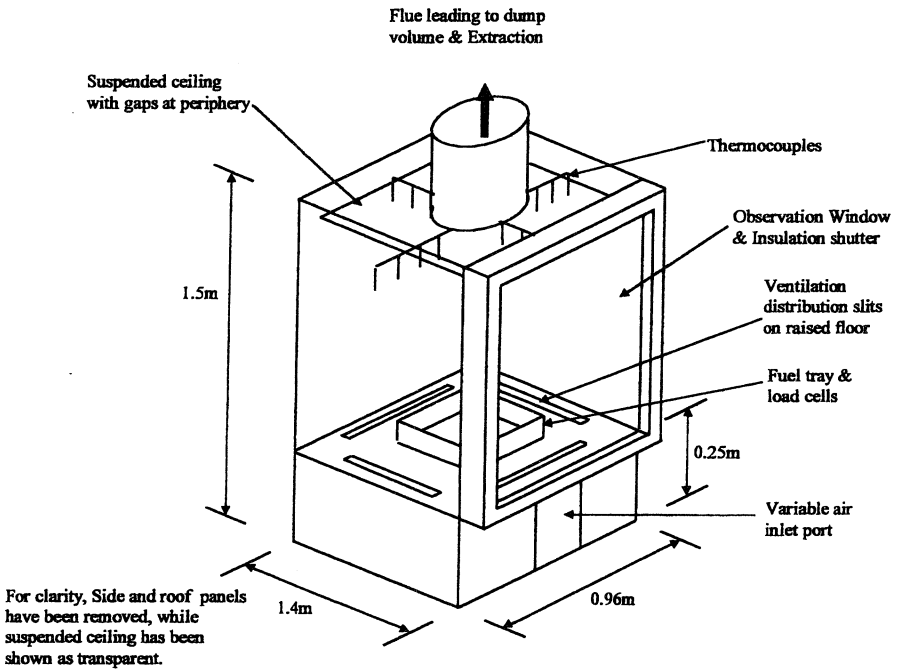

Fig.1. Schematic diagram of experimental investigation rig.

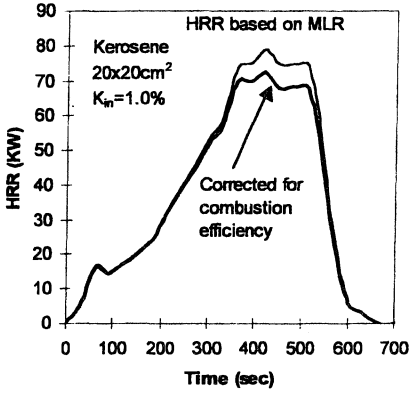

Fig.2. Heat release rate based on the mass-loss rate as a function of time, for the largest air inlet area.

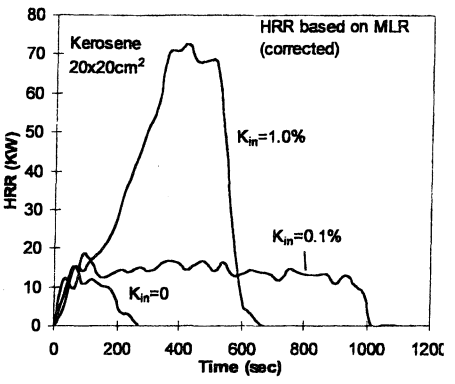

Fig.3. Heat release rate based on the mass-loss rate (corrected for combustion efficiency)as a function of time for the different air inlet area coefficients (K_{in})

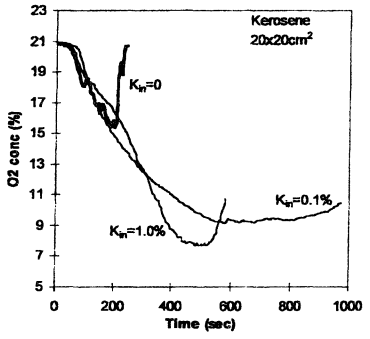

(a)

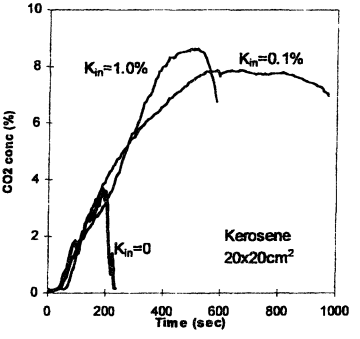

(b)

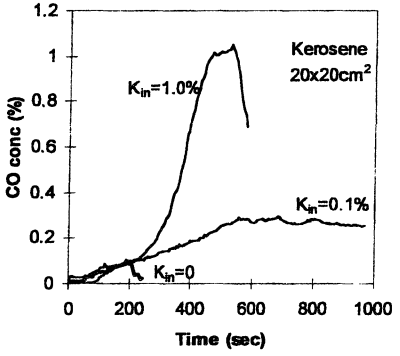

(c)

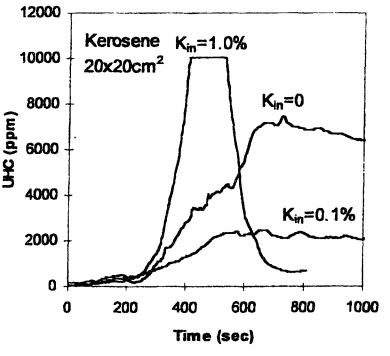

(d)

Fig. 4. Fire gas composition analysis as a function of time for the different air inlet area coefficients (K_{in}). (a) Oxygen, (b) carbon dioxide, (c) carbon monoxide, (d) unburnt hydrocarbons

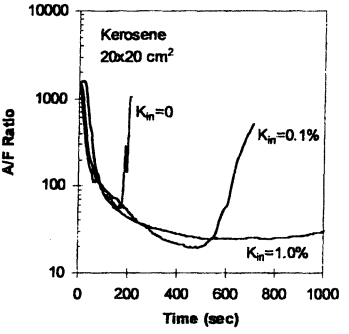

Fig.5. Calculated A/F ratio from gas analysis as a function of time for the different air inlet area coefficients (K_{in})

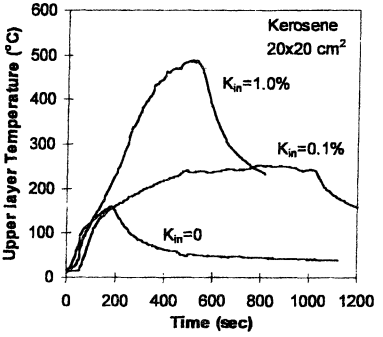

Fig. 6. Average hot layer temperature as a function of time for the different air inlet area coefficients (K_{in})

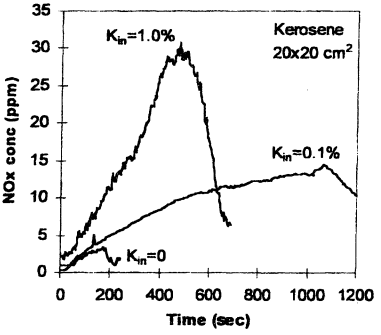

Fig.7. NOx concentration measurements as a function of time, for the different air inlet area coefficients (K_{in})

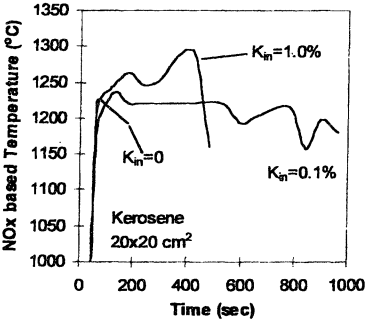

Fig.8. Calculated temperature based on rate of NOx formation as a function of time for the different air inlet area coefficients (K_{in})

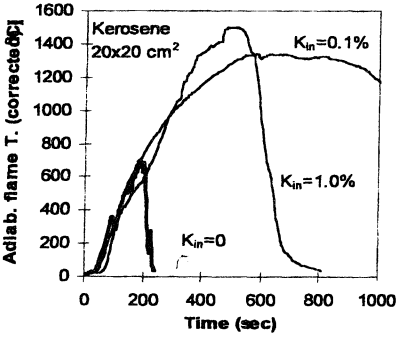

Fig.9. Calculated adiabatic flame temperature corrected for efficiency as a function of time for the different air inlet area coefficients (K_{in})

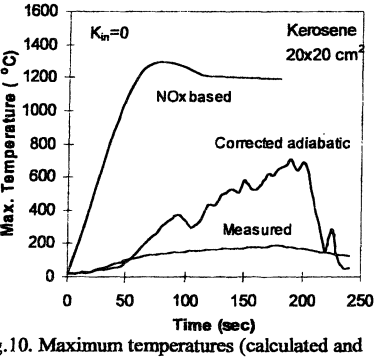

Fig.10. Maximum temperatures (calculated and measured) as a function of time for K_{in}=0

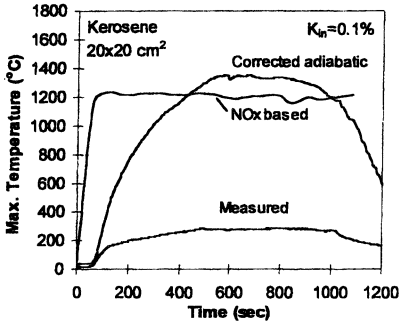

Fig.11. Maximum temperatures (calculated and measured) as a function of time for K_{in}=0.1%

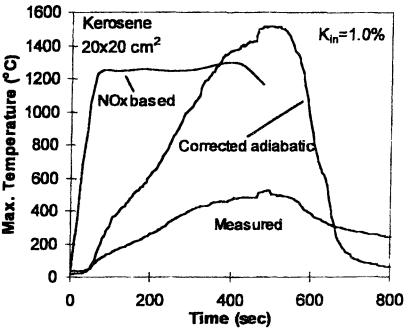

Fig.12. Maximum temperatures (calculated and measured) as a function of time for K_{in}=1.0%

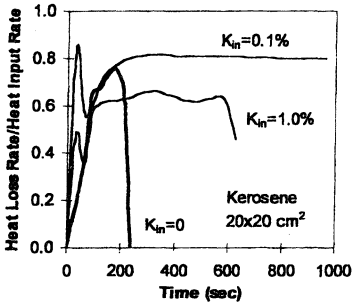

Fig.13. Ratio of heat loss to heat input rate as a function of time for the different air inlet area coefficients (K_{in})

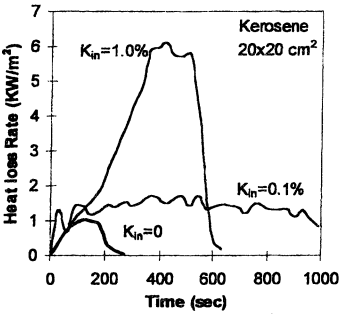

Fig.14. Heat loss rate per unit area as a function of time for the different air inlet area coefficients (K_{in})